Published in : Journal of Materials Chemistry (2010)
Status : Postprint (Author's version)

Preparation of fire-resistant poly(styrene-co-acrylonitrile) foams using the supercritical CO_2 technology

Laetitia Urbanczyk,[a] Serge Bourbigot,[b] Cédric Calberg,[c] Christophe Detrembleur,[a] Christine Jérôme,*[a] Frédéric Boschini,[d] and Michaël Alexandre[a]

[a] *Center for Education and Research on Macromolecules (CERM), University of Liège, Sart-Tilman B6a, 4000 Liège, Belgium. Fax: +32 43663497; Tel: +32 43663491, E-mail: C.Jerome@ulg.ac.be*

[b]*Equipe Procédés d'Elaboration de Revêtements Fonctionnels, LSPES, UMR-CNRS 8008, ENSCL, BP 90108, 59652 Villeneuve d'Ascq, Cedex, France*

[c]*Department of Applied Chemistry, University of Liège, Sart-Tilman B6a, 4000 Liège, Belgium*

[d]*Laboratoire de Chimie Inorganique Structurale, University of Liège, Sart-Tilman B6a, 4000 Liège, Belgium*

Abstract

This work deals with the preparation and characterization of fire-resistant poly(styrene-co-acrylonitrile) (SAN) foams containing (organo)clays and/or melamine polyphosphate (MPP) as fire retardants using supercritical CO_2 as the foaming agent. The additives dispersion was first characterized with X-ray and transmission electron microscopy (TEM) analyses. Their presence clearly affected the cellular morphology, as observed by scanning electron microscopy (SEM). Then, the peak of heat release rate (PHRR) and total heat evolved (THE) were determined with cone calorimetry test, performed on each foamed sample as a function of the foam density. Incorporation of clay (3 and 5wt%) in the exfoliated state into SAN foam clearly led to a significant decrease of PHRR, while intercalated and aggregated clay had a lower effect. Similar results were obtained with 10 and 20wt% of MPP. The best results were obtained when exfoliated clay and MPP were combined, with a PHRR drop as large as 75%, thanks to the synergistic action of both additives. The magnitude of PHRR drop, related to the fire resistance, was found to be in direct relationship with the cohesiveness of the protective carbonaceous layer formed at the sample surface during combustion. Clay and MPP, when added together, are thus believed to favour the formation of a highly cohesive protective layer able to act as an efficient shield against the flame, despite the fact that the sample is originally composed of ~90% of voids.

Introduction

Polymeric foams are widely used materials in various domains like upholstered furniture and automotive or for isolation purposes. Although many polymers are foamed with chlorofluorocarbons (CFCs), these physical foaming agents tend to be replaced by more environmentally friendly gases due to their high reactivity towards the Earth's protecting ozone layer. In Europe, CFCs are extensively substituted by n- and cyclopentane because of their zero ozone depletion potential (ODP), low cost and high availability. However,

these gases tend to worsen the fire behaviour of the foams[1]. CO_2 is another acceptable alternative to CFCs due to its much lower ODP. Furthermore, this gas is non flammable, making it very attractive for purposes where low flammability is an important issue. Another specificity of this particular gas is its ability to produce microcellular foams[2-4], i.e. foams with cell size lower than 100µm and cell density higher than 10^8cells/cm³, in contrast to classical blowing agents where cell size usually exceeds 100µm. These microcellular foams are attractive because they are characterized by higher mechanical resistance compared to their macrocellular counterparts. This very interesting property opens the market of polymeric foams to a lot of applications where plain materials can be replaced by lighter – and thus cheaper – ones, without suffering much of resistance loss. These advantages have driven our choice towards this promising blowing agent.

Poly(styrene-co-acrylonitrile) (SAN) has been selected for its ease of foaming with $scCO_2$ and its well-known degradation mechanism during combustion[5]. SAN foams are used in sandwiched panels especially in marine environment and also as decorative interior mouldings. The extensive use of polymeric foams in housing applications has raised questions about safety issue concerning those highly flammable materials. In fact, these foams are basically composed of hydrocarbons full of voids, and their thermal inertia is very low, making them prone to fast combustion. Thus, commercial styrenic foams are classically filled with brominated fire retardants in order to improve their fire behaviour[6]. Nowadays, the research on new flame retardants aims not only at decreasing the flammability of the material, but also at limiting the amount of smoke and at replacing halogenated compounds by more environmentally friendly and safer additives[7]. Potential alternatives include metal hydroxides, phosphorus- and nitrogen-based compounds including intumescent systems, ... But to be efficient, these additives must usually be used at high loadings (20-50wt%) and their presence can adversely affect the polymer foamability as well as foam mechanical properties. Nowadays, nanometric fillers attract an increasing interest in the area of polymer resistance to fire. When introduced in polymer matrices, they exhibit good fire resistance effectiveness at very low level (<10wt%) thanks to the high specific area they can develop when adequately dispersed. In that context, expandable graphite[8,9], carbon nanofibers[10], talc and nanoclay[11] have been envisaged as potential alternatives to halogenated compounds into polyurethane foams. It has been demonstrated that expandable graphite at 15-25wt% loading or 4wt% carbon nanofibers in combination with a brominated flame retardant lowered significantly the foam flammability. Those assessments have been highlighted by the use of cone

calorimetry, which is one of the most classical methods to characterize materials burning behaviour at laboratory scale[12,13], allowing to determine important values such as the peak of heat release rate (PHRR) or the total heat evolved (THE) during the experiment.

The group of Wilkie[14] has evidenced the relationship between the maximum extent of PHRR drop achievable and the polymer degradation mechanism. During sample combustion, the clay accumulates at the surface and forms a protective layer between the material and the flame. The lamellar filler acts also as gas barrier which impedes the diffusion of the degradation products towards the flame, allowing more time for radical recombination. Indeed, two additional degradation pathways of SAN have been evidenced in the presence of nanoclay using GC/MS analysis. This kind of additive thus acts exclusively in the condensed phase.

Even if polymer/clay nanocomposites greatly reduce the PHRR, these materials still fail to pass regulatory fire safety tests, like UL94, which are qualitative and more specific for the targeted application[15,16]. In fact, the nanocomposite burns slowly but does not self-extinguish, and the whole sample is thus combusted. Following some specialists, nanoclays are very promising fire retardants when combined with other retardants in order to pass these tests[15]. In fact, some synergistic effects have already been evidenced between nanoclays and several flame retardants, as reviewed by Morgan[15].

The present study aims at characterizing the fire behaviour of poly(styrene-co-acrylonitrile)/clay nanocomposite foams prepared with supercritical fluid technology. A few works report on the beneficial effect of 3-5 wt% of nanoclay on SAN flammability with a PHRR drop from 30 to 50%[5,14,17,18]. From these observations, similar trends are expected for SAN nanocomposite foams. SAN/clay nanocomposites with different clay dispersion levels have been prepared with the use of commercial clays or home-made pre-exfoliated clay composed of poly(ε-caprolactone) chains grafted from the clay surface. The goal of these experiments is to highlight the importance of clay delamination degree into SAN polymeric foams on their burning behaviour improvement. The second part of the paper focuses on melamine polyphosphate (MPP) as fire retardant. Its efficiency is first compared with nanoclays, and then both additives are combined in order to investigate possible synergistic effects in reaction to fire.

To the best of our knowledge, this is the first report dealing with the quantitative investigation of the combustion behaviour of polymeric foams prepared with the supercritical fluid technology.

Experimental

Materials

Poly(styrene-*co*-acrylonitrile) (SAN) with an AN content of 25wt% has been supplied by BASF (Luran®358N, 1.08 g.cm^{-3}). The commercial (organo)clays, Cloisite® Na^+ (CNa) and Cloisite® 30B (C30B), come from Southern Clay Products. They are made of aluminosilica-based lamellar sheets stacked together. CNa is natural (100wt% in inorganics) and C30B is organo-modified with 20wt% of bis-(2-(hydroxyethyl)methyl) (tallowalkyl)ammonium cation (80wt% in inorganics). Home-made pre-exfoliated organoclay, MB30B, was also used in this study. This filler contains 53wt% of inorganic clay, 13wt% of the same ammonium as Cloisite® 30B and 34wt% of poly(ε-caprolactone) chains mainly grown from the ammonium hydroxyl groups. The preparation of this highly filled pre-exfoliated clay, also called masterbatch, was undergone in supercritical CO_2 in order to take advantage of this unusual polymerization medium. All the details about its synthesis and characterization can be found in a previous paper[19]. Melamine polyphosphate (MPP) (Melapur® 200, purity 95%, 1.85 g.cm^{-3}) was provided by Ciba. CO_2 was supplied by Air Liquide Belgium (purity 99.95%) and used as received.

Foams preparation

SAN/clay nanocomposites were prepared by melt blending the clay (C30B) or PCL/clay masterbatch (MB30B) with the polymer in a twin-screw Brabender® static mixer at 175°C for 5 minutes with a roller blade rotation speed of 60rpm. The inorganic content is set at 3 or 5wt%. The same procedure is applied to prepare SAN/MPP and SAN/clay/MPP composites, keeping the total flame retardant content (inorganics from clay + MPP) at 10 or 20wt%. CNa was dispersed into SAN in a continuous twin-screw extruder adapted to allow water injection. Details about this method can be found in a previous paper[20].

Nanocomposite foams have been prepared according to the following procedure in order to obtain foamed samples of required dimensions for cone calorimetric measurements. The melt blended samples were moulded into 2mm-thick samples in a hot press (175°C) for 5 minutes, followed by cutting with a circular saw in order to obtain ready-to-foam 63 x 70 x 2mm^3 sheets. The nanocomposite sheet is then placed vertically in a 250ml high pressure vessel and left to soak for 22h at 60°C under 120bar of CO_2 (under these conditions, CO_2 is in the supercritical state). After rapid depressurisation (~10s), the sample is quickly removed from the vessel and placed between two pre-heated metallic

sheets and the system is dipped in a 110°C silicone bath to allow foaming. The foam is then quenched in an ice/water bath for 10 minutes and washed with toluene and paper towels to remove the oil from the sample surface. The foams are finally cut into 10x10cm^2 sheets for cone calorimetry tests. Foams of different density have been obtained by adjusting the foaming time from 30s to 5min. With this foaming process, the foam thickness oscillates between 5 and 7mm.

Characterization methods

X-ray diffraction analysis (XRD) was carried out with a powder diffractometer Siemens D5000 (Cu K_α radiation with λ = 0.15406 nm, 50 kV, 40 mA, Ni filter, $\theta/2\theta$ geometry) at room temperature for 2θ varying from 1.65° to 30° by 0.04° steps, in order to characterize the final nanocomposites morphology. Clay delamination efficiency was directly observed by transmission electron microscopy (TEM, Philips CM100). Ultrathin sections (50-80 nm) were prepared with an Ultramicrotome Ultracut FC4e, Reichert-Jung. No staining was used since the aluminosilicate sheets are contrasting enough in the polymer matrix.

The cellular structure of the foams was observed by scanning electron microscopy (SEM; JEOL JSM 840-A) after metallization with Pt. Image analysis was manually performed on the basis of SEM pictures by measuring the size of at least 100 cells. Cell density (N_{cell}) was estimated according to the following formula: $N_{cell} = (n\ M^2/A)^{3/2}.d^{-1}$, where n is the number of cells in the SEM picture, M the magnification, A the surface area of the picture (cm^2) and d the foam density ($g.cm^{-3}$).

Combustion behaviour was assessed according to the ASTM E 906 procedure in a Fire Testing Technology Limited Instruments mass loss cone calorimeter. The equipment is identical to that used in oxygen consumption cone calorimetry (ASTM E-1354-90), except that a thermopile in the chimney is used to measure heat release rate (HRR) rather than employing the oxygen consumption principle. Mass loss readings are performed simultaneously following the ASTM E-1354 norm, and serve as a benchmark of the heat release rate values obtained in this manner. The measurements have been performed at a heat flux of 35kW.m^{-2}, using a cone shaped heater. The foams (100 x 100 x 5-7 mm^3) in horizontal orientation were subjected to a spark until the sample was ignited. The aim was to simulate the conditions likely to occur in a real fire (small fire scenario). When measured at 35kW.m^{-2}, HRR is reproducible to within <10%.

The residues obtained after mass loss cone calorimetry test were analyzed by ^{31}P and ^{27}Al solid state NMR. Measurements were conducted using a Bruker Avance II 400

spectrometer (static field 9.4 T) operating at a Larmor frequency of 161.98 MHz for ^{31}P. ^{31}P spectra were performed using a 4-mm probe. Ground samples were packed in 4mm fused zirconia rotors and sealed with Kel-F caps. Spectra were recorded at 10 kHz spinning rate at the magic angle (MAS) with high-power ^{1}H decoupling using single pulse

Table 1 Characteristics of the nanocomposites to be foamed

Sample	Clay type	Total inorganic content /wt%	Interlayer distance [c] /nm	Nanocomposite morphology
SAN	No filler	0	-	-
SAN/3CNa [a]	Cloisite® Na^+	3	1.1	Disaggregated, but not intercalated
SAN/3C30B [b]	Cloisite® 30B	3	3.5	Mainly intercalated
SAN/3MB30B [b]	MB30B	3	Weak signal	Mainly exfoliated
SAN/5MB30B [b]	MB30B	5	Weak signal	Mainly exfoliated

[a] Nanocomposite prepared by water extrusion process[20].

[b] Nanocomposite prepared by melt blending.

[c] Determined by XRD analysis.

acquisition with a recycle delay of 300 s. Typically, 32 scans were necessary to obtain spectra with good signal to noise ratio. H_3PO_4 at 85% in water was used as reference. Solid state NMR of ^{27}Al was performed at 208.49 MHz on Bruker Avance II 800 spectrometer operating at 18.8 T with MAS at 20 kHz. Bruker probe heads equipped with 3.2 mm rotor assembly were used with the same type of rotors described above. A recycle delay of 10s was used for all samples. The reference used was a saturated solution of $Al(OH)_3$.

Results and discussion

1. SAN/clay nanocomposite foams

1.1 Nanocomposites preparation and foaming

Several kinds of clays and mixing methods have been used in order to reach different degrees of nanoclay dispersion into SAN (Table 1). The details about the preparation method as well as complete characterization of the nanocomposites can be found in previous works[20,21]. Transmission electron microscopy (TEM) pictures and X-ray diffractograms of these samples can be found in Electronic Supplementary Information (ESI)[†]. As the natural clay CNa has very poor affinity with SAN, a new mixing method involving water injection in an extruder has been used in order to help clay de-aggregation[20]. Water is automatically removed from the sample during venting. The resulting composite is translucent, but no polymer intercalation occurs, according to X-ray diffraction.

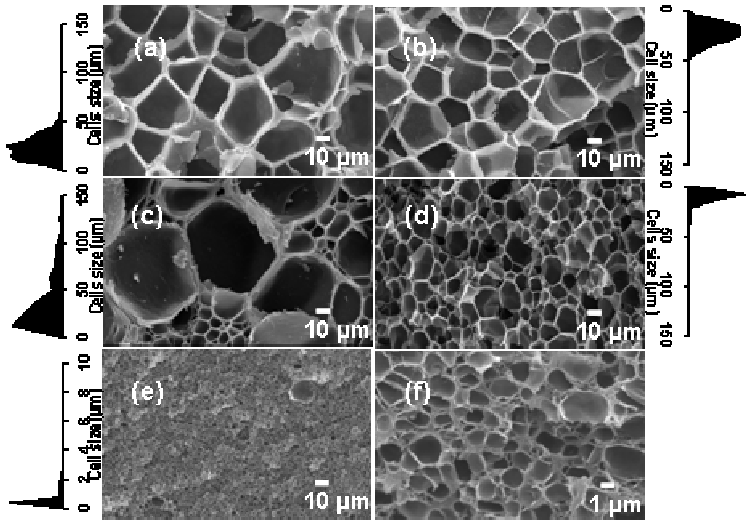

Fig. 1 SEM microphotographs and cell size distribution of SAN and SAN/clay foams prepared with $scCO_2$: (a) SAN, (b) SAN/3CNa, (c) SAN/3C30B, (d) SAN/3MB30B, (e) SAN/5MB30B, (f) SAN/5MB30B at higher magnification.

TEM analysis reveals a homogeneous dispersion of small clay stacks about 50nm-thick (Figure S1a)[†]. Thus, the clay in SAN/3CNa is highly disaggregated, thanks to favourable interactions with the water injected, but no polymer is intercalated. In contrast, C30B

simply mixed with SAN in an internal mixer leads to intercalated nanocomposite (Figure S1b)†, thanks to the good affinity of SAN for this kind of clay[17,22,23]. Polymer intercalation is confirmed by XRD analysis with an increase of the interlayer distance from 1.8 nm (C30B) to 3.5 nm (Table 1, Figure S2†). Some stacks remain optically visible in the sample, attesting for imperfect clay dispersion in SAN/3C30B. In order to improve Cloisite® 30B dispersion into SAN, a home-made masterbatch, MB30B, has been used in this work. This masterbatch, also called pre-exfoliated clay, is made of poly(ε-caprolactone) (PCL) chains in-situ intercalated/grafted between the Cloisite® 30B sheets.

The XRD signal is very weak for the samples obtained upon melt dispersion of MB30B into SAN (Figure S2)†. This result attests for a mainly exfoliated morphology, although some small stacks, composed of 2 to 6 sheets, still remain. TEM characterization of these samples confirms the morphological assumptions made on the basis of XRD analysis (Figure S1c,d)†. We assume that foaming the nanocomposite does not influence its exfoliation state on the basis of the work of Okamoto[24], who evidenced nanoplatelets orientation along cell walls and disorganized exfoliation in the cell struts, without any sign of clay re-aggregation.

Pure SAN as well as SAN/clay nanocomposites have been foamed using supercritical CO_2. Before focussing on the fire properties of those foams, their morphology is first assessed. Scanning electron microscopy (SEM) pictures of the foamed nanocomposites are presented in Figure 1 with the corresponding cell size distribution curves, while cell density values can be found in Table S1†. As can be seen in Figure 1a, pure SAN foam is characterized by regular cellular structure, with pores diameter around 20-70µm. When some nanoclay is added, SAN porosity is influenced differently depending on the degree of platelets delamination. In fact, nanoclay is well-known for its heterogeneous nucleating ability in polymer foaming[25], its efficiency being essentially dependent on its specific surface area (directly related to its delamination level in the polymer) and on the foaming conditions. Thus, at similar clay content and foaming conditions, the cellular structure of SAN/3CNa (lowest specific surface area) remains nearly unaffected (Figure 1b), while SAN/3MB30B has smaller cells (5-20µm) with a narrowed cell size distribution (Figure 1d) compared to unfilled SAN foam (20-70µm). Indeed, this sample is characterized by the best extent of nanoclay delamination (highest specific surface area).

The effect is even more pronounced at 5wt% clay loading, with pores size as low as 0.2-4µm due to the higher particle loading (Figure 1e,f). Cell density of SAN foam progressively increases in accordance with the finer clay dispersion level, attesting for the

Table 2 Cone calorimetric data of SAN and SAN/clay nanocomposite foams.

Foamed sample	Density range ($g.cm^{-3}$)	Ignition time (s)	Average PHRR ($kW.m^{-2}$)	S. d. PHRR[a]	Average THE ($kW.m^{-2}$)	S. d. THE[a]
SAN	0.11-0.13	50	254	36	14.4	1.9
	0.13-0.15		258	45	17.6	2.4
	0.15-0.17		276	39	21.4	4.4
SAN/3CNa	0.11-0.13	50	198	47	14.2	0.5
	0.13-0.15		204	12	17.1	1.1
	0.15-0.17		263	64	19.8	2.3
SAN/3C30B	0.11-0.13	39	169	24	12.3	0.2
	0.13-0.15		183	31	14.2	0.6
	0.15-0.17		188	-[b]	17.6	-[b]
SAN/3MB30B	0.11-0.13	30	152	7	15.2	2
	0.13-0.15		146	4	14.5	4.2
	0.15-0.17		136	-[b]	16.3	-[b]
SAN/5MB30B	0.11-0.13	27	117	51	12	4.3
	0.13-0.15		142	22	16	3.2
	0.15-0.17		134	29	15	3.4

[a] Standard deviation associated with the PHRR or THE value in the investigated density range.

[b] No repetition has been performed for this density range.

heterogeneous nucleating ability of the clay (Table S1)[†]. Concerning SAN/3C30B, its porous structure is bimodal, with big cells around 50-100µm surrounded by smaller cells of 10-20µm (Figure 1c). Large cells are believed to result from nucleation at clay stacks surface due to gas accumulation at the clay/polymer interface, whereas smaller ones must come from smaller intercalated particles. The same kind of observation is made for SAN/5MB30B (Figure 1e,f), with sub-micrometric cells (0.5-1µm) surrounding cells of 2-4µm. The cell size is thus largely decreased at 5wt% clay loading compared to 3wt%. Smaller cells are believed to nucleate near exfoliated clay platelets while the slightly bigger cells could result from residual intercalated clay sheets. It must be noted that attempts to foam nanocomposites containing more than 5wt% of MB30B with our

foaming process failed due to the excessively high viscosity of the nanocomposite at such high clay content.

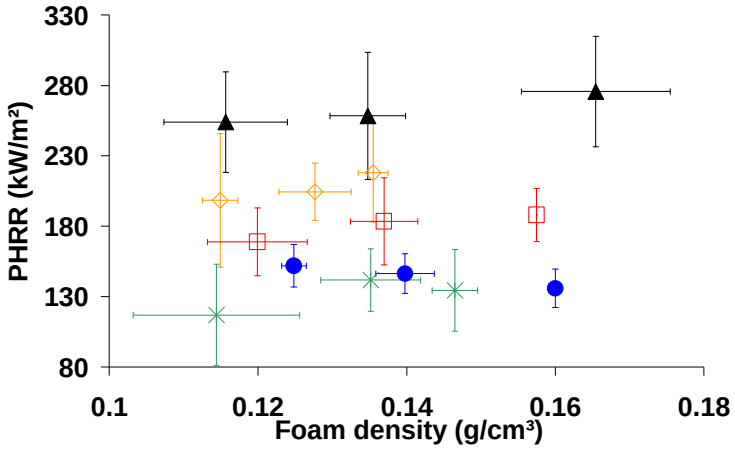

Fig. 2 Peak of heat release rate (PHRR) of SAN and SAN/clay foams, measured with cone calorimetry: (▲) SAN, (◊) SAN/3CNa, (□) SAN/3C30B, (●) SAN/3MB30B, (✳) SAN/5MB30B. Error bars for PHRR takes into account both standard deviation over the measures and the 10% systematic error.

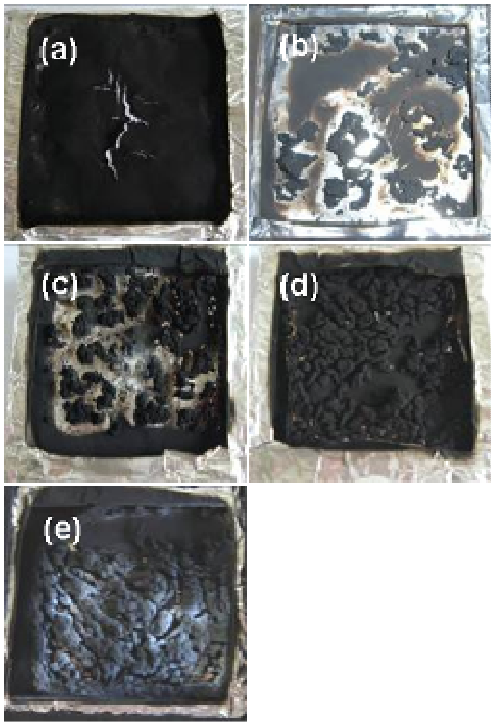

Fig. 3 Pictures of the residues recovered after cone calorimetry tests performed on SAN and SAN/clay nanocomposite foams : (a) SAN, (b) SAN/3CNa, (c) SAN/3C30B, (d) SAN/3MB30B, (e) SAN/5MB30B.

1.2 Mass loss calorimetry test

Mass loss calorimetry measurements are presented in the form of peak of heat release rate (PHRR) versus foam density. According to Zammarano, the cellular structure has no significant influence on PHRR value of foams having similar density (at least in the density range investigated, i.e. 0.14-0.17 g/cm³)[11]. Thus, we assume that our foams may be compared despite their different cellular morphology. The density of the foams prepared in the present study varies from 0.11 to 0.17 g/cm³ depending on the foaming time allowed and experimental error associated with density determination.

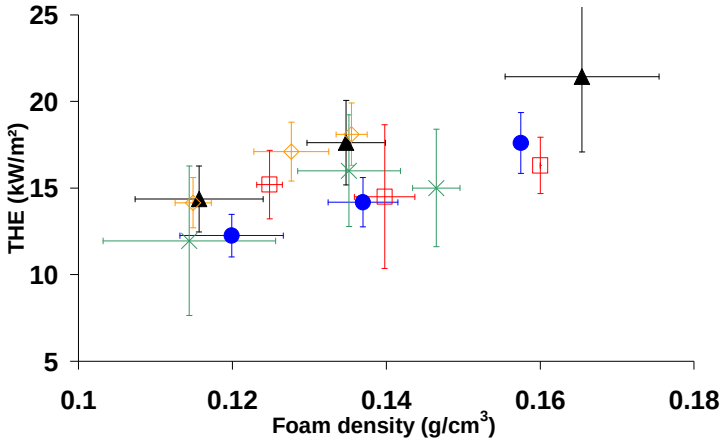

Fig. 4 Total heat evolved (THE) of SAN and SAN/clay foams, measured with cone calorimetry : (▲) SAN, (◊) SAN/3CNa, (□) SAN/3C30B, (●)SAN/3MB30B, (✳) SAN/5MB30B. Error bars for THE takes into account both standard deviation over the measures and the 10% systematic error.

Cone calorimetric results related to SAN and SAN/clay nanocomposite foams are presented in Figures 2-4 and gathered in Table 2. Some typical HRR curves in function of time can be found in ESI (Figure S3)[†]. For each kind of sample, the PHRR is reported as a function of the foam density at three different density ranges. The vertical error bars have been calculated from repetitions of PHRR measurements performed in the selected density range (standard deviation). PHRR value of SAN, SAN/3CNa and SAN/3C30B foams increases progressively with the foam density. This result is consistent with the higher amount of matter burned. This tendency is less obvious for SAN/MB30B foams. This different behaviour is rather surprising, but we suggest that for a given foam composition, a similar protective layer is formed whatever the foam density in the investigated density

range. This would explain the nearly invariable PHRR drop when SAN nanocomposites based on exfoliated organoclays are concerned.

As a general trend, SAN/clay nanocomposite foams are characterized by lower average PHRR compared to pure SAN foam (Figure 2). The magnitude of PHRR drop appears to be highly dependent on the extent of nanoclay delamination level inside the foam. In fact, the curves related to exfoliated nanocomposite foams are below the intercalated one, while the non intercalated Cloisite Na^+ leads to the lowest PHRR drop. The PHRR is similar at 3 and 5wt% of exfoliated clay loading. It seems that a plateau has been reached.

Considering those results and the pictures of Figure 3, a link can be made between the magnitude of PHRR drop and the aspect of the carbonaceous char formed during the combustion test. In fact, while the carbonaceous char of SAN/3C30B (Figure 3c) is distributed in individual islands, SAN/3MB30B (Figure 3d) covers more homogeneously the surface, even tough many cracks prevents its full cohesiveness.

The most cohesive residue is obtained with SAN/5MB30B (Figure 3e). Oppositely, such carbonaceous residue is almost nonexistent in SAN/3CNa sample (Figure 3b). Char formation during polymer/lamellar clay combustion has already been extensively

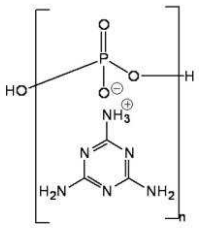

Fig. 5 Chemical structure of melamine polyphosphate.

described in the literature[13]. During combustion, the nanofiller accumulates at the sample surface. The layer formed both physically protects the material from the flame and slows down the diffusion of degradation products, allowing more time for radical recombination. The more cohesive char limits the degradation of foams and forms an efficient insulative barrier at the surface of the material. This explains the very good fire performance of the foams containing only a few percent of very well-dispersed nanoclays. Furthermore, the total heat evolved, or THE, is decreased by about 10-20% in average in the case of nanocomposite foams based on organomodified clays (Figure 4). Thus, some polymer decomposition product is "trapped" in the carbonaceous char or transformed into char. This phenomenon has already been observed in other works[26,27]. In contrast, THE of

SAN/CNa remains similar to SAN foam due to the lack of char cohesiveness.

Apart from PHRR and THE values, cone calorimetry analysis give also access to the time to ignition, i. e. the time needed for the sample to ignite under the heat source. We observed a decrease of the time to ignition for all the nanocomposites (27-50s) compared to neat polymer foam (50s, see Table 2). Faster ignition is typical for this kind of nanoclay-filled material[28]. In fact, the heat is less easily dissipated in such highly viscous materials (accumulation of heat at the surface of the material due to lower heat conductivity compared to virgin foam) and as a consequence, it concentrates in a local region, inducing faster local thermal degradation and anticipated ignition.

2. MPP-containing SAN foams

2.1 Foams preparation

In several works, nanoclays are used in combination with another flame retardant in order to lower the total amount of additive needed, thanks to synergistic effects[16]. In the present study, the beneficial effect of melamine polyphosphate (Figure 5) on SAN foam burning behaviour is first assessed. In a second step, MPP and nanoclay are combined in order to investigate potential synergistic effect. MPP is already a combination of two flame retardants, a nitrogenated and a phosphorylated one, working in a synergistic way[28]. In fact, both of them act in a different way to protect the sample against fire. On one side, the main degradation pathways of the nitrogenated compound involve the release of melamine which can condense and form nitrogenated heterocyclic compounds, while it can also decompose endothermically with the release of ammonia and water as inert gases, thus cooling and diluting the flame. On the other side, phosphorus-containing molecules produce phosphoric acid upon decomposition. This acid catalyses char formation and forms a protective layer on the sample surface. When those two components are combined, their concomitant action reaches higher effectiveness than each component alone.

Table 3 Composition of SAN composites containing nanoclay (MB30B) and/or melamine polyphosphate (M).

Foamed sample[a]	MPP content /wt%	Nano clay content /wt%	Total additive content /wt%	Interlay distance /nm[b]	Nanocomp. morphology[c]
SAN/10M	10	0	10	-	-
SAN/20M	20	0	20	-	-
SAN/7M/ 3MB30B	7	3	10	3.5 (Weak Signal)	Mainly exfoliated
SAN/17M/ 3MB30B	17	3	20	3.5 (Weak Signal)	Mainly exfoliated
SAN/5M/ 5MB30B	5	5	10	3.4 (Weak Signal)	Mainly exfoliated

[a] SAN/xM with x=wt% of MPP and SAN/xM/yMB30B with x=wt% of MPP and y=wt% of inorganic content from MB30B.

[b] Determined with XRD analysis.

[c] Estimated from XRD and TEM analyses.

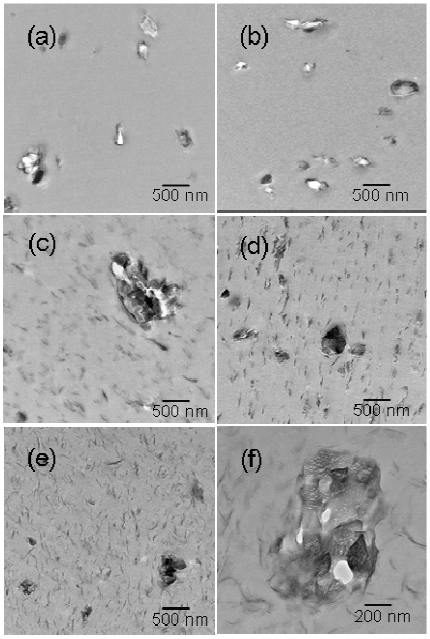

Fig. 6 TEM analysis of SAN/MPP and SAN/MPP/clay composites: (a) SAN/10M, (b) SAN/20M, (c) SAN/7M/3MB30B, (d) SAN/5M/5MB30B, (e) SAN/17M/3MB30B, (f) SAN/5M/5MB30B at higher magnification.

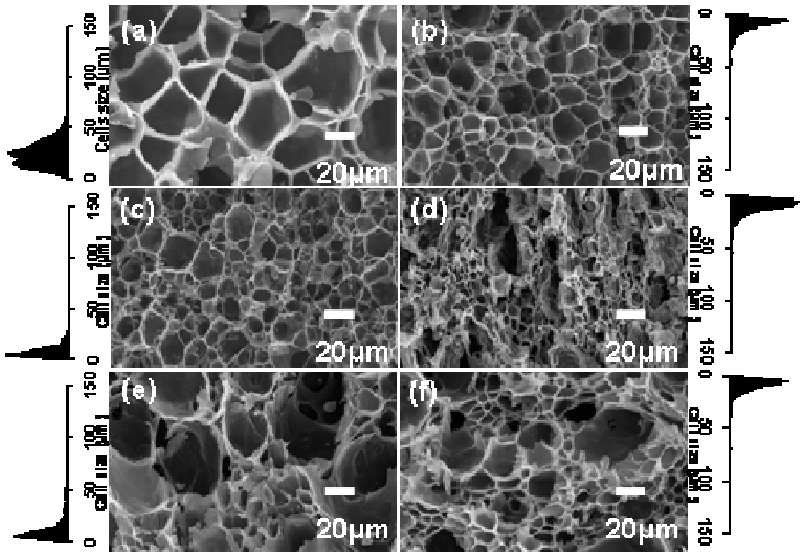

Fig. 7 SEM microphotographs and cell size distribution of SAN, SAN/MPP and SAN/MPP/clay foams prepared with $scCO_2$: (a) SAN, (b) SAN/10M, (c) SAN/20M, (d) SAN/7M/3MB30B, (e) SAN/17M/3MB30B, (f) SAN/5M/5MB30B.

This specific system has been chosen in the frame of this study because it already proved its efficiency in other systems like in bulk HIPS[29] or bulk PU[30]. In practical, a few binary and tertiary composites containing 10 and 20wt% of additives have been prepared, with different clay/MPP mutual proportions in the case of ternary blends. The composition of these samples is summarized in Table 3. First, melamine polyphosphate distribution into SAN is evaluated by transmission electron microscopy. This micrometric additive seems to be homogeneously distributed throughout the polymer and the nanocomposites (Figure 6a-e).

In the case of ternary blends, some nanoclay platelets are found around melamine polyphosphate particles (Figure 6f). This particular organization reflects an interaction between those two additives. It is interesting to investigate the effect of this kind of organization on the ternary blend fire resistance. It must be stressed that the state of nanoclay dispersion is not affected by micrometric MPP additives, as observed by TEM and confirmed by XRD analysis (Table3 and Figure S4[†]).

The above-mentioned binary and ternary blends are then foamed with $scCO_2$. As can be observed in Figure 7, melamine polyphosphate addition has an influence on the SAN foam morphology. In fact, smaller cells (2-25µm) are observed at 10wt% MPP loading, with a similar cellular structure than SAN/3MB30B. Increasing MPP content to 20wt% only increases the proportion of small cells, while keeping the same range of cells size. From

these experiments, it is clear that solid melamine polyphosphate particles also act as heterogeneous nucleating sites, even though their efficiency is clearly poorer than nanometric clay fillers. In fact, only 3wt% of nanoclay results in equivalent amount of cells than 20wt% of micrometric melamine polyphosphate ($5\ 10^9$ and $4.3\ 10^9$ cells.cm^{-3} respectively, Table S1[†]). Some works devoted to polymer foaming report about the critical parameters governing the heterogeneous nucleation efficiency of different kinds of fillers[31,32]. They conclude that the specific surface area, surface curvature as well as

Table 4 Cone calorimetric data of SAN/M and SAN/M/clay foams.

Foamed sample	Density range (g.cm^{-3})	Ignition time (s)	Average PHRR (kW.m^{-2})	S. d. PHRR[a]	Average THE (kW.m^{-2})	S. d. THE[a]
SAN	0.11-0.13	50	254	36	14.4	1.9
	0.13-0.15		258	45	17.6	2.4
	0.15-0.17		276	39	21.4	4.4
SAN/10M	0.11-0.13	28	150	-[b]	11.5	-[b]
	0.13-0.15		151	18	13	2.3
	0.15-0.17		152	24	14	2
SAN/20M	0.11-0.13	40	114	16	10.4	2.2
	0.13-0.15		130	7	12.3	1.6
	0.15-0.17		140	-[b]	12.8	-[b]
SAN/7M/3MB30B	0.11-0.13	48	128	12	10.5	1
	0.13-0.15		132	9	11.8	0.8
	0.15-0.17		130	11	13.2	0.2
SAN/17M/3MB30B	0.11-0.13	53	88	3	8	0.3
	0.13-0.15		105	22	9.9	1.7
	0.15-0.17		106	-[b]	10.3	-[b]
SAN/5M/5MB30B[c]	0.13-0.15	45	104	-[b]	10.7	-[b]
	0.15-0.17		129	10	14.3	1

[a] Standard deviation associated with the PHRR or THE value in the investigated density range.

[b] No repetition has been performed for this density range.

[c] We were unable to prepare SAN/5M/5MB30B foams of low density (0.11-0.13 g.cm^{-3}) due to too high nanocomposite viscosity.

filler/polymer/gas nature and foaming conditions have an influence on their effectiveness.

In our case, the specific surface is believed to be the determining parameter.

When both additives are added, the cell size distribution broadens, with big cells surrounded by smaller ones. The porous morphology is thus a little bit different than SAN/3MB30B and SAN/10M. This difference might be explained by different nucleating abilities of free nano- and microfillers and of the MPP additive surrounded by clay platelets. Attempts to foam SAN/30M or SAN/15M/5MB30B failed, due to restricted expansion related to higher sample viscosity (foams density > 0.25g.cm^{-3}). These samples would not have been comparable to the other ones and, as a consequence, were not taken into account in the present study.

2.2 Mass loss calorimetry test

Fire performance of these foams has been evaluated by mass loss calorimetry and the results are presented in Table 4. Some representative HRR curves can also be found in Figure S5†. SAN/melamine polyphosphate foams are first discussed. The effectiveness of such additive as fire retardant is clearly demonstrated for this kind of foam. In fact, PHRR of pure SAN foams drops by around 40% with only 10wt% of MPP and this drop reaches 50% at 20wt% MPP loading. The PHRR values obtained with 10 and 20wt% of MPP are very similar to those achieved with respectively 3 and 5wt% of nanoclay based on MB30B. This means that, on a weight fraction basis, exfoliated nanoclays seem to be more efficient than melamine polyphosphate in reducing the amount of heat released during combustion. Indeed, only a low amount of well-dispersed nanometric filler is required to build the protective layer responsible for reduced PHRR. Furthermore, the thin platelet morphology of the nanometric filler facilitates the formation of a cohesive layer at the sample surface. These oriented flat particles also impede very effectively gas diffusion thanks to good gas barrier properties[33]. The total amount of heat evolved (THE) during SAN foam combustion is reduced by 10-20% upon the addition of 3-5wt% of nanoclay and it drops by 30-40% with MPP (Table 4). This result can be related to some polymer trapped in the carbonaceous char.

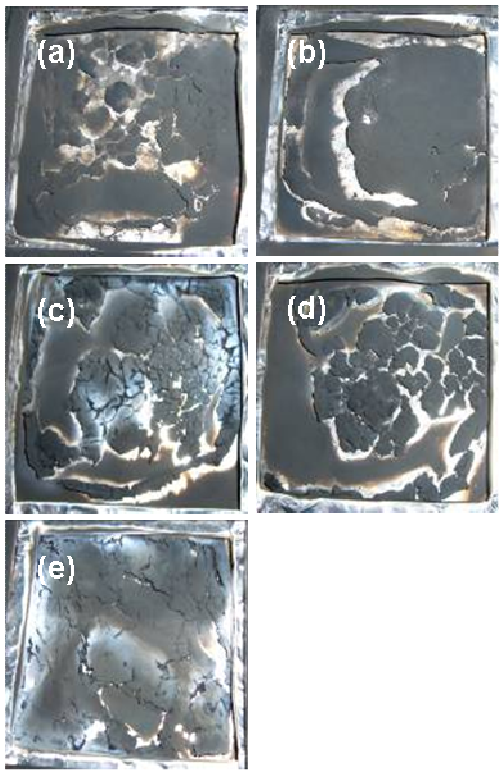

Fig. 8 Pictures of the residues recovered after cone calorimetry tests performed on SAN/MPP and SAN/MPP/clay foams: (a) SAN/10M, (b) SAN/20M, (c) SAN/7M/3MB30B, (d) SAN/17M/3MB30B, (e) SAN/5M/5MB30B.

The last part of the study focuses on fire performance of ternary blend foams, where a fraction of melamine polyphosphate has been replaced by nanoclay (MB30B).

At 10wt% additive loading, fire performance of SAN/10M foam is enhanced when some clay replaces melamine polyphosphate. It can thus be stated that melamine polyphosphate and nanoclay act in a synergistic way because at same additive loading, fire performance is higher when both fillers are combined. The effect is more pronounced at 5/5wt% M/clay proportion than at 7/3wt%. The same trend is observed for foams containing a total additive loading of 20wt%. In fact, PHRR of SAN/20M drops by around 15-20% when 3wt% of melamine-based additive is replaced by nanoclays.

Those results highlight a synergistic behaviour between nanoclay and melamine polyphosphate. As mentioned earlier, nanoclay only influences the combustion mechanism in the condensed phase. Thus, the synergistic behaviour must originate from the formation of a more homogeneous protective layer during combustion, thanks to the combination

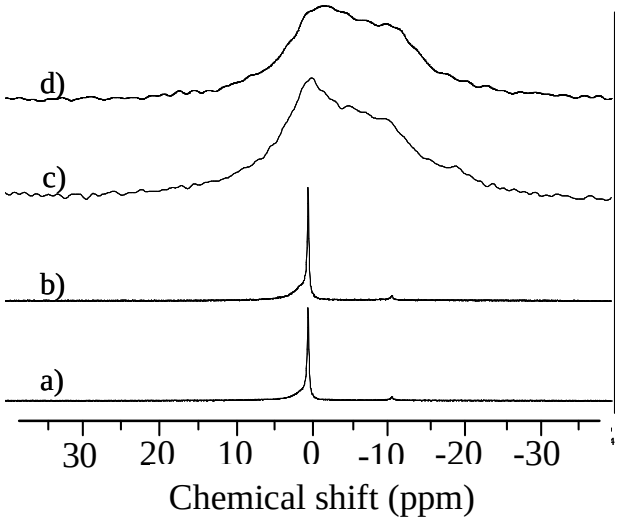

Fig. 9 MAS ^{31}P NMR spectra of a-b) SAN/20M foams and c-d) SAN/17M/3MB30B foams. For each sample, a repetition is made at slightly different foam density: a) 0.13 g.cm^{-3}, b) 0.15 g.cm^{-3}, c) 0.13 g.cm^{-3}, d) 0.14 g.cm^{-3}.

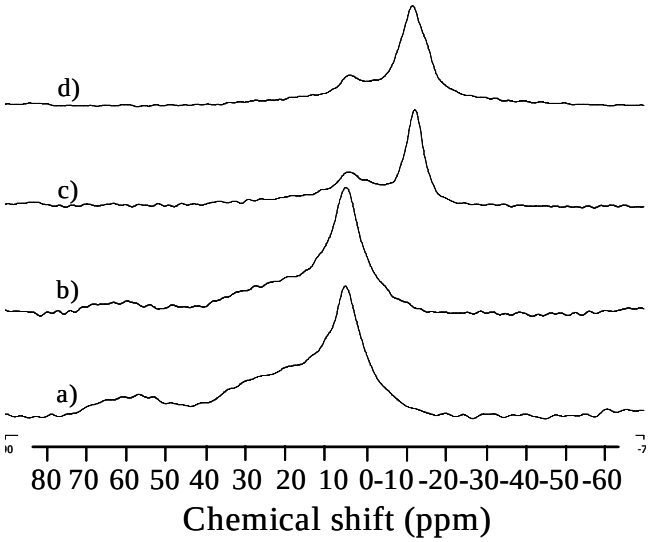

Fig. 10 MAS ^{27}Al NMR spectra of a-b) SAN/3MB30B foams and c-d) SAN/17M/3MB30B foams. For each sample, a repetition is made at slightly different foam density: a) 0.13 g.cm^{-3}, b) 0.14 g.cm^{-3}, c) 0.13 g.cm^{-3}, d) 0.14 g.cm^{-3}.

of different mechanisms of flame retardancy. Figure 8 shows the aspect of the carbonaceous layers recovered after the burning tests. It can be observed that melamine polyphosphate alone forms a partially cohesive flat residue. When 3wt% of nanoclay is added in combination with melamine polyphosphate, some parts of the char become thicker and form non cohesive islands of aggregates, surrounded by the flat residue typical

of melamine polyphosphate. At 5wt% loading, nanoclay is able to form a thick and highly cohesive char, rather smooth on the top. It looks like melamine polyphosphate has filled many of the cracks present on SAN/5MB30B foam residue (Figure 8e). While the THE of SAN was decreased by around 10-40% for the binary blend foams (Table 4), the effect is more pronounced for the ternary blend foams with a THE drop reaching up to 50% in the case of SAN/17M/3MB30B, due to the highly cohesive coating formed. Thus, we can affirm on the basis of PHRR curves and the aspect of the residues that melamine polyphosphate and nanoclay, when added together, act in synergy to reduce greatly the amount of heat released during foam combustion thanks to the highly effective carbonaceous coating formed at the surface of the sample.

In a former work, Bourbigot *et al* have suggested the formation of an aluminophosphate ceramic structure upon reaction between the clay and ammonium polyphosphate (APP)[34]. This assumption was made on the basis of solid state NMR analysis performed after thermal treatment of EVA/PA6-clay nanocomposite/APP at several temperatures. But in other works, the same group observed that no reaction occurs between MPP and Cloisite® 30B when dispersed in a PA6 matrix, based on a complete study of the system composed of aluminum phosphinate-melamine polyphosphate (Exolit O1311 from Clariant)[35,36] and Cloisite® 30B used as fire retardant for PA6. In that particular system, the clay actually improves the char efficiency by promoting the nucleation of a high density of small closed cells in the char, thus decreasing the apparent thermal conductivity of the protective layer and increasing the char cohesiveness. In light of these findings, we performed SEM, ^{31}P and ^{27}Al NMR analyses on some mass loss calorimetry residues to elucidate the mecanism(s) of resistance to fire. SEM analysis reveals a foam-like char structure for SAN/MB30B and SAN/MPP/MB30B residues (Figure S6)[†], indicating the formation of a char with improved thermal insulation (foamed structures are known to have weaker thermal conductivity). Figure 9 shows MAS NMR ^{31}P spectra of four cone residues. In the case of sample containing only MPP, a sharp band is observed at 0 ppm exhibiting a shoulder at about 1 ppm which can be assigned to orthophosphate groups linked to aliphatic groups and/or orthophosphoric acid[37]. An additional small band shows up at -11 ppm which can be assigned to pyrophosphate species and/or to diphenylorthophosphate groups[38]. When clay is incorporated in the formulation, a broad band is observed lying from 15 to -35 ppm. This linewidth is due to a continuous distribution of ^{31}P isotropic chemical shifts reflecting the structural disorder such as bond angle and bond length

variations and higher coordination sphere disorder[39]. This behavior may be due to the formation of phosphate-type glasses.

Figure 10 shows MAS NMR ^{27}Al spectra of four cone residues. The spectra of the SAN/3MB30B residues (without MPP) exhibit broad bands centered at 56 ppm and 5 ppm, which can be assigned to Al in tetrahedral and octahedral coordination, respectively[40,41]. A shoulder centered at 25 ppm can be also distinguished and is assigned to $[AlO_5]$ unit[42,43]. When 17% MPP are incorporated in the formulation, two bands are distinguished at 3 and -13 ppm. Compared to the two previous spectra, it is noteworthy that the peak positions are displaced to higher fields. This is because of the presence of phosphorous within the second sphere of coordination. This P has a marked effect upon the peak position of AlOx units; which shifts from 5 ppm for $Al[OAl]_6$ to -13 ppm for $Al[OP]_6$ and from 56 ppm $Al[OAl]_4$ to 3 ppm for $Al[OP]_4$[44,45]. This proves, therefore, that the clay can react with MPP to form aluminophosphates. From these experiments, we can affirm that the foam-like char residue and the aluminophosphates formed during combustion both contribute to very effective protective layer able to significantly reduce the amount and rate of heat released during combustion.

Conclusion

SAN as well as SAN/clay, SAN/MPP and SAN/MPP/clay composites have been successfully foamed with supercritical CO_2. The cellular structure is found to be in direct relationship with the specific surface area of the filler, while more irregular foams are obtained when both types of additives are mixed together. The combustion behaviour of SAN/clay nanocomposite foams has first been assessed with cone calorimetry. PHRR values are found to slightly increase with the sample weight, and to decrease progressively as the extent of nanoclay delamination, or clay content, increases. The magnitude of PHRR drop is put in relation with the cohesiveness of the carbonaceous char formed during combustion, which impedes gas diffusion and acts as a physical shield against the flame. The second part of the study was devoted to SAN/melamine polyphosphate fire behaviour. Similarly to well-dispersed nanoclays, PHRR values decreased also by 40 up to 50% with the addition of 10 and 20% of MPP into SAN foams. Those results are related to both the carbonaceous char formed and the inert gases (water and ammonia) released during combustion which cools the flame. Synergy between nanoclay and MPP has been highlighted in the ternary blend foams containing both kinds of additives. The highest

PHRR drop, 75%, is observed for SAN/17M/3MB30B sample whose residue is the most cohesive. It is suggested that the improved char cohesiveness might result from a) the nanoclay acting as a nucleating agent, leading to a porous char structure, b) the formation of aluminophosphates as evidenced by NMR analysis, and c) MPP producing a flat protective layer filling the cracks in the char like those found when only nanoclay was used.

Acknowledgements

CERM is grateful for the financial support from the "Interuniversity Attraction Poles" Programme PAI P6/27 - Belgian State - Belgian Science Policy and from the "Région Wallonne" for its financial support in the frame of the WINNOMAT program: PROCOMO. The authors thank CAT-μ "Cellule d'appui technologique en microscopie" of the University of Liège for giving access to XRD equipment. C.D. is "Senior Research Associate" by F. R. S.-FNRS, Belgium. The authors are indebted to Mr. Bertrand Revel of the common research NMR center of the University of Lille 1for skilful technical assistance in NMR experiment and for helpful discussion.

References

1 Z. Tang, M. Maroto-Valer, J. W. Andresen, J. Miller, M. L. Listemann, P. L. McDaniel, D. K. Morita and W. R. Furlan, *Polymer*, 2002, **43**, 6471-6479.

2 D. L. Tomasko, H. Li, D. Liu, X. Han, M. J. Wingert, L. J. Lee and K. W. Koelling, *Ind. Eng. Chem. Res*, 2003, **42**, 6431-6456.

3 D. L. Tomasko, A. Burley, L. Feng, S.-K. Yeh, K. Miyazono, S. Nirmal-Kumar, I. Kusaka and K. W. Koelling, *J. Supercritical Fluids*, 2009, **47**, 493-499.

4 L. J. M. Jacobs, M. F. Kemmere and J. T. F. Keurentjes, *Green Chem.*, 2008, **10**, 731-738.

5 B. N. Jang, M. Costache and C. A. Wilkie, *Polymer*, 2005, **46**, 10678-10687.

6 E. D. Weil and S. V. Levchik, *J. Fire Sci.*, 2007, **25**, 241-265.

7 J. Q. Wang and W. K. Chow, *J. Appl. Polym. Sci.*, 2005, **97**, 366-376.

8 M. Modesti, A. Lorenzetti, F. Simioni and G. Camino, *Polym. Degrad. Stab.*, 2002, **77**, 195-202.

9 M. Modesti and A. Lorenzetti, *Eur. Polym. J.*, 2003, **39**, 263-268.

10 M. Zammarano, R. H. Kramer, R. Harris, T. J. Ohlemiller, J. R. Shields, .S. S. Rahatekar, S. Lacerda, S. and J. W. Gilman, *Polym. Adv. Technol.*, 2008, **19**, 588-595.

11 M. Zammarano, J. W. Gilman, R. H. Kramer, R. Harris, T. J. Ohlemiller, and J. R. Shields, Effect of nanoparticles on flammability of flexible polyurethane foams. *Recent advances in flame retardancy of polymeric materials.*(Proceedings of **19th BCC Conference**) Stamford, CT, 2008.

12 J. W. Gilman, *Appl. Clay Sci.*, 1999, **15**, 31-49.

13 F. Laoutid, L. Bonnaud, M. Alexandre, J. M. Lopez-Cuesta, and P. Dubois, *Mater. Sci. Eng. R*, 2009, **63**, 100-125.

14 B. N. Jang, C. A. Wilkie, *Polymer*, 2005, **46**, 9702-9713.

15 A. B. Morgan, *Polym. Adv. Technol.* 2006, **17**, 206-217.

16 S. V. Levchik and E. D. Weil, *Polym. Int.*, 2008, **57** , 431-448.

17 H. A. Stretz, M. W. Wootan, P. E. Cassidy and J. H. Koo, *Polym. Adv. Technol.*, 2005, **16**, 239-248.

18 J. Zhang, D. D. Jiang, D. Wang, and C. A. Wilkie, *Polym. Degrad. Stab.*, 2006, **91**, 2665-2674.

19 L. Urbanczyk, C. Calberg, F. Stassin, M. Alexandre, R. Jérôme, C. Jérôme, C. Detrembleur, *Polymer*, 2008, **49**, 3979-3986.

20 M. Mainil, L. Urbanczyk, C. Calberg, A. Germain, C. Jérôme, S. Bourbigot, J. Devaux, M. Sclavons, *Polym. Eng. Sci*., 2009, Accepted for publication.

21 L. Urbanczyk, C. Calberg, S. Benali, S. Bourbigot, E. Espuche, F. Gouanvé, P. Dubois, A. Germain, C. Jérôme, C. Detrembleur and M. Alexandre, *J. Mater. Chem.* , 2008, **18** , 4623-4630.

22 L.-L. Chu, S. K. Anderson, J. D. Harris, M. W. Beach, and A. B. Morgan, *Polymer*, 2004, **45**, 4051-4061.

23 H. A. Stretz and D. R. Paul, *Polymer*, 2006, **47**, 8123-8136.

24 M. Okamoto, P. H. Nam, P. Maiti, T. Kotaka, T. Nakayama, M. Takada, M. Ohshima, A. Usuki, N. Hasegawa and H. Okamoto, *Nano Lett*., 2001, **1**, 503-505.

25 L. J. Lee, C. Zeng, X. Cao, X. Han, J. Shen, and G. Xu, *Compos. Sci. Technol.*, 2005, **65**, 2344-2363.

26 J. Zhu, A. B. Morgan, F. J. Lamelas and C. A. Wilkie, *Chem.Mater.*, 2001, **13**, 3774-3780.

27 F. Dabrowski, M. Le Bras, L. Cartier and S. Bourbigot, *J. Fire Sci.*, 2001, **19**, 219-240.

28 S. V. Levchik, L. Costa and G. Camino, *Polym. Degrad. Stab.*, 1994, **43**, 43-54.

29 U. Braun and B. Schartel, *J. Fire Sci.*, 2005, **23**, 5-30.

30 L. Song, Y. Hu, Y. Tang, R. Zhang, Z. Chen, and W. Fan, *Polym. Degrad. Stab.*, 2005, **87**, 111-116.

31 N. H. Fletcher, *J. Chem. Phys.*, 1958, **29**, 572-576.

32 S. N. Leung, A. Wong, C. B. Park, J. H. Zong, *J. Appl. Polym. Sci.*, 2008, **108**, 3997-4003.

33 R. K. Bharadwaj, *Macromolecules*, 2001, **34**, 9189-9192.

34 S. Bourbigot, M. Le Bras, F. Dabrowski, J. W. Gilman and T. Kashiwagi, *Fire Mater.*, 2000, **24**, 201-208.

35 F. Samyn, Ph. D. Thesis, ENSCL, Lille (France), 2007.

36 S. Bourbigot, F. Samyn, T. Turf, and S. Duquesne, *Polym. Degrad. Stab.*, 2009, In Press.

37 T. M. Duncan, D. C.Douglass, *J. Chem. Phys*. 1984, **87,** 339.

38 S. Bourbigot, M. Le Bras, R. Delobel, R. Descressain, J. P.Amoureux, *J Chem Soc Faraday Trans*, 1996, **92**, 149.

39 F. Fayon, D. Massiot, K. Suzuya, D. L. Price, *J. Non-Cryst. Solids*, 2001, **283**, 88

40 E. R. H. Van Eck, A. P. M. Kentgens, H. Kraus, R. Prins, *J. Phys. Chem.*, 1995, **99**, 16080.

41 S. J. Duffy, G. W. Van Loon, *Can. J. Chem.*, 1995, **73**, 1645.

42 J. J. Fitzgerald G. Piedra S. F. Dec M. Seger G. E. Maciel *J. Am. Chem. Soc.*, 1997, **119**, 7832.

43 T. J. Bastow, C. Jaeger G. Kunath-Fandrei M. E. Smith, *Bull. Magn. Res.*, 1996, **17**, 250.

44 D. Mueller, G. Berger, I. Grunze, G. Ladwig, E. Hallas, C. Haubenreisser, *Phys. Chem. Glasses*, 1983, **24**, 37.

45 S. Bourbigot, M. Le Bras, R. Delobel, J. M. TreHmillon, *J. Chem. Soc. Faraday Trans.*, 1996, **92**

Published in : Journal of Materials Chemistry (2010)
Status : Postprint (Author's version)

Supplementary data

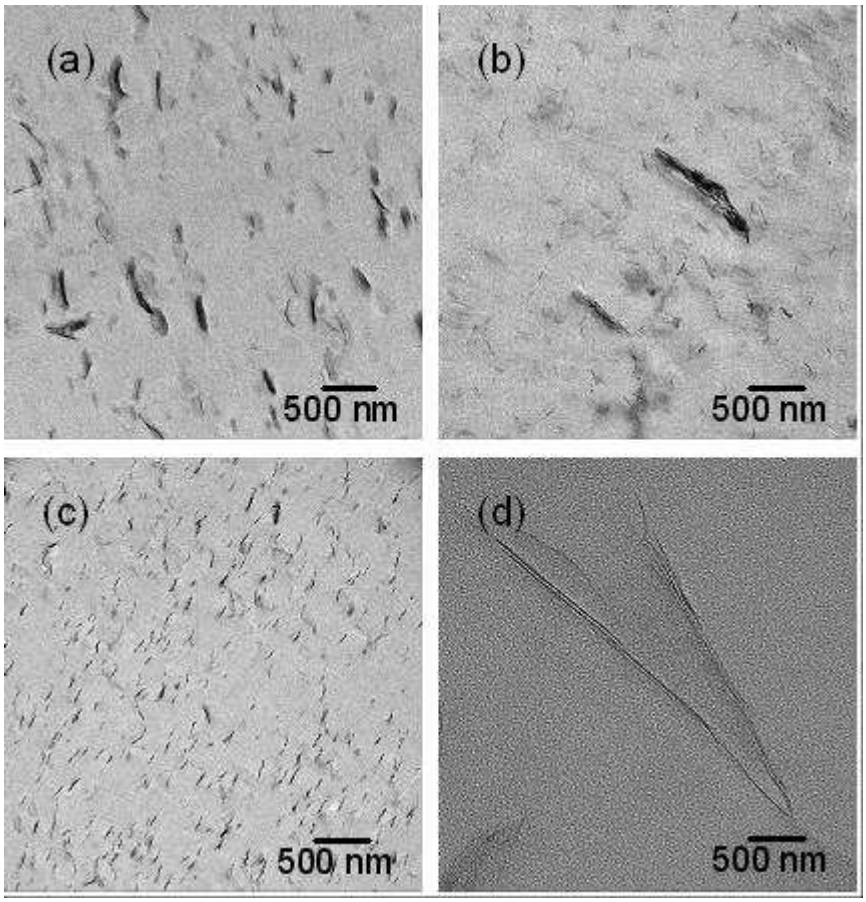

Fig. S1 TEM analysis of SAN/clay nanocomposites: (a) SAN/3CNa, (b) SAN/3C30B, (c) SAN/3MB30B, (d) SAN/3MB30B at higher magnification.

Published in : Journal of Materials Chemistry (2010)
Status : Postprint (Author's version)

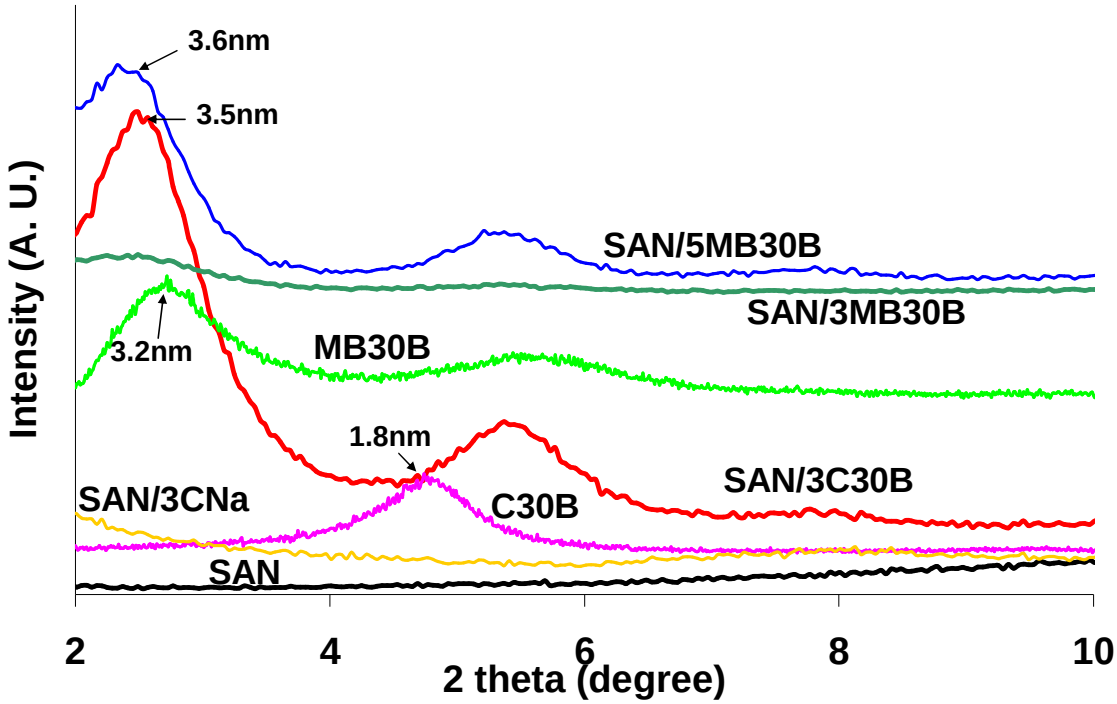

Fig S2 XRD patterns of clays and SAN/clay nanocomposites.

Published in : Journal of Materials Chemistry (2010)
Status : Postprint (Author's version)

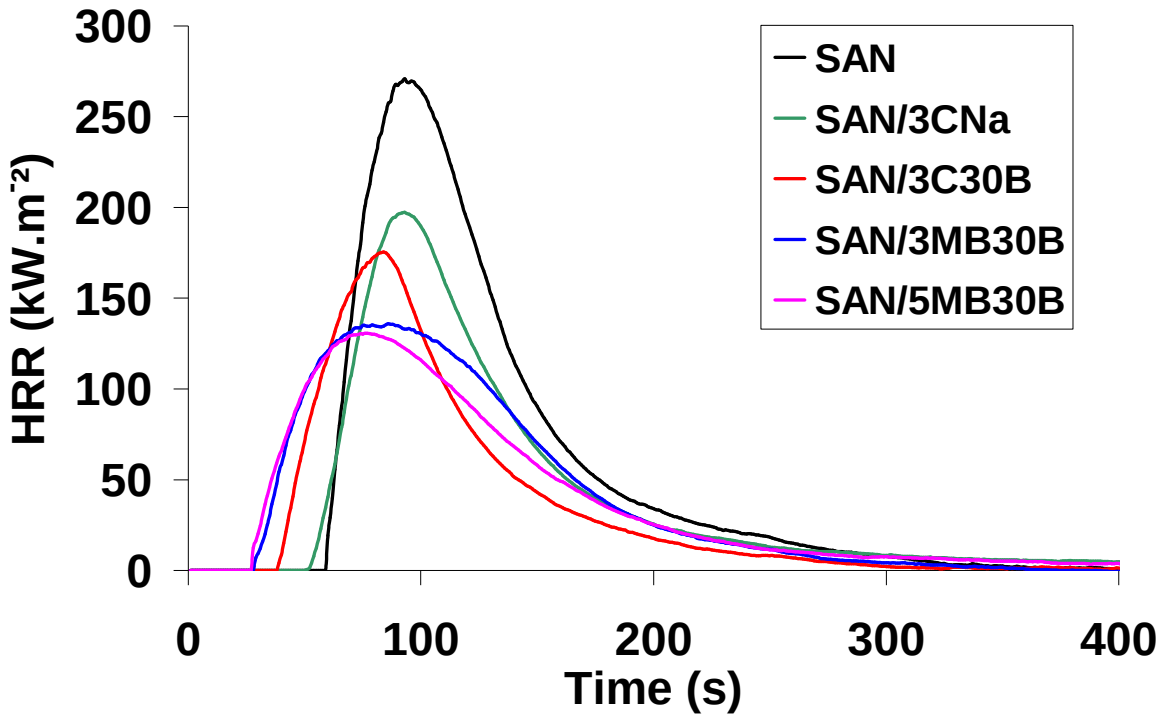

Fig. S3 Heat release rate (HRR) plots of SAN and SAN/clay nanocomposite foams at 35kW.m^{-2} heat flux in the 0.13-0.15g.cm^{-3} density range.

Published in : Journal of Materials Chemistry (2010)
Status : Postprint (Author's version)

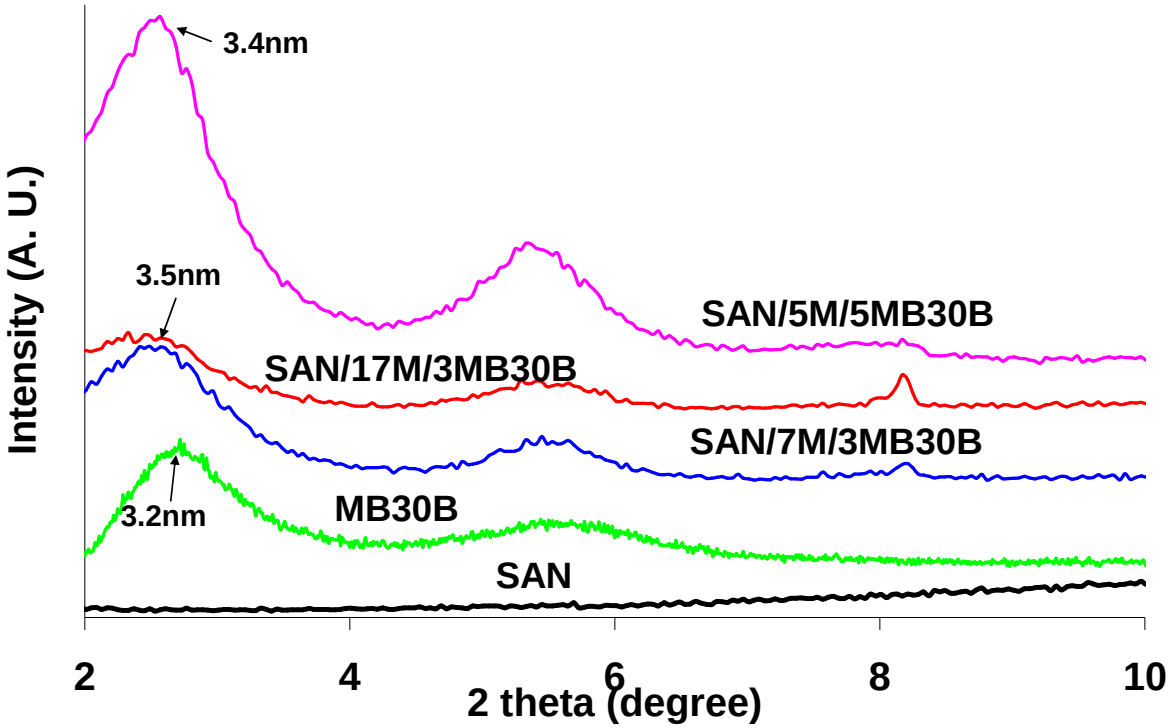

Fig. S4 XRD patterns of SAN/MPP/clay nanocomposites.

Published in : Journal of Materials Chemistry (2010)
Status : Postprint (Author's version)

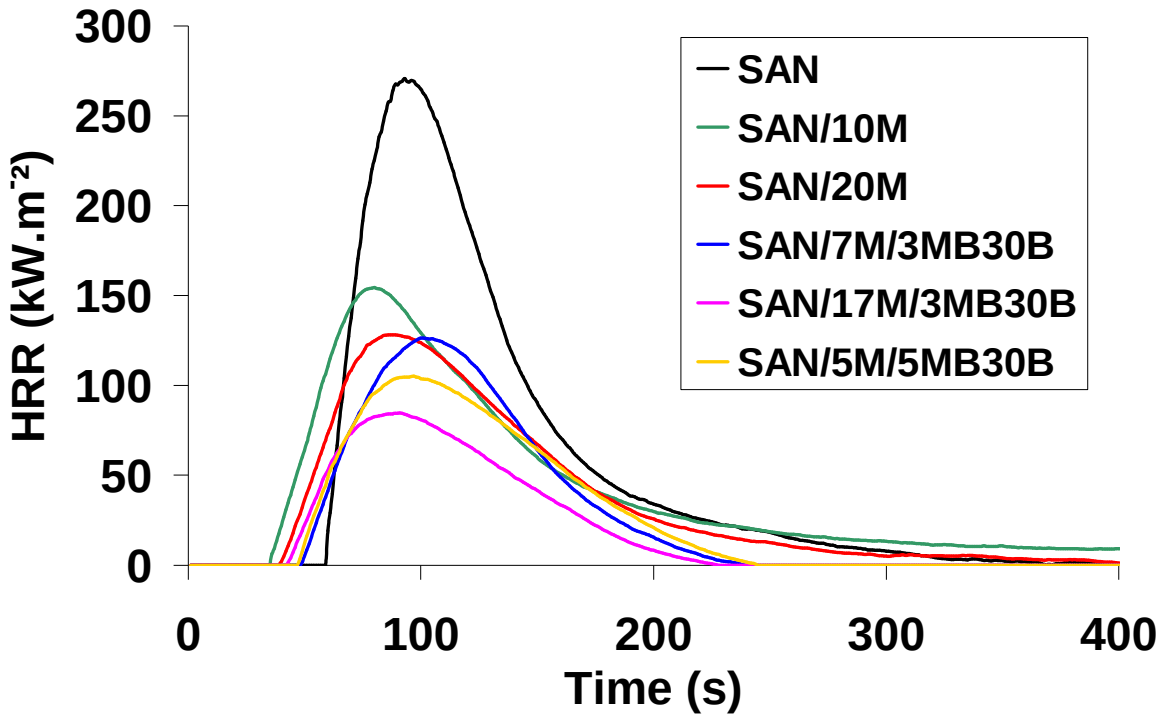

Fig. S5 Heat release rate (HRR) plots of SAN/MPP and SAN/MPP/clay nanocomposite foams at 35kW.m^{-2} heat flux.

Published in : Journal of Materials Chemistry (2010)
Status : Postprint (Author's version)

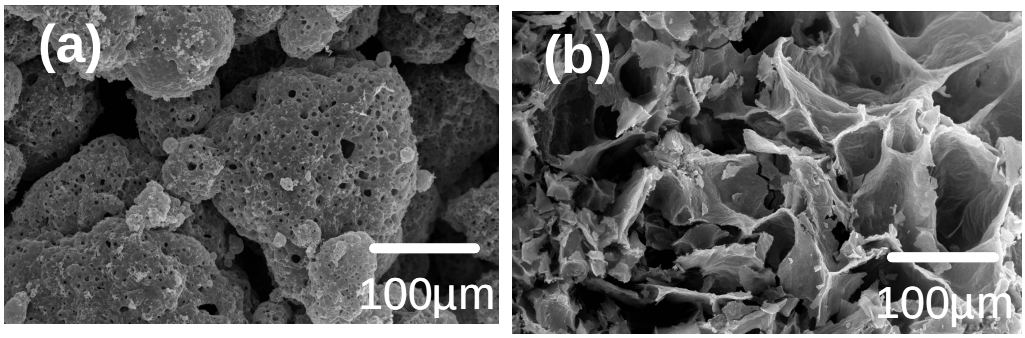

Fig. S6 SEM pictures of the foam-like char obtained after cone calorimetry test : a) SAN/3MB30B, b) SAN/5M/5MB30B.

Published in : Journal of Materials Chemistry (2010)
Status : Postprint (Author's version)

Foamed sample	Cell size range (µm)	Cell density (10^{-8} cells.cm^{-3})
SAN	20-70	2.5
SAN/3CNa	10-40	5.2
SAN/3C30B	10-100	0.8
SAN/3MB30B	2-20	50
SAN/5MB30B	0.2-4	15000
SAN/10M	2-25	26
SAN/20M	2-20	43
SAN/7M/3MB30B	5-40	13.5
SAN/17M/3MB30B	5-50	13
SAN/5M/5MB30B	5-70	22

Table S1 Cell size and cell density of SAN, SAN/clay, SAN/MPP and SAN/MPP/clay nanocomposite foams.